Collision-induced dissociation mechanisms in 4.83-keV H_3^+-He collisions

O. Yenen and D. H. Jaecks
Behlen Laboratory of Physics, University of Nebraska, Lincoln, Nebraska 68588-0111
(Received 11 October 1983; revised manuscript received 20 February 1985)

The polarization of L_α radiation is measured in coincidence with the scattered H_2^+ resulting from the collision process: $H_3^+ + He \rightarrow (H_3^+)^* + He \rightarrow H_2^+ + H(n=2) + He$ for specific laboratory angles. Our results are interpreted within the quasidiatomic approximation, which provides a reasonable picture of the changing nodal structure of the wave function during the collision. Within this description, the excitation is dependent upon the orientation of the molecule relative to the beam direction.

I. INTRODUCTION

In recent years, we have witnessed an increased trend toward the investigation of more and more complex systems. In atomic and molecular collision physics, this trend is manifested by trying to describe the collisions of ions, atoms, or molecules with molecules by multidimensional correlation surfaces.[1] Since this task becomes highly complicated, even for relatively simple molecules, a simpler model would be most welcome to estimate the qualitative dynamical behavior of molecular collisions. The collision models incorporating quasidiatomic correlation diagrams[1,2] seem to be a good candidate despite their simple approach to the problem. However, we need to empirically establish their range of applicability to different systems. This paper explores the possibilities of extending the basic ideas used to describe the excitation of diatomic systems to more complicated molecules by investigating the collision-induced dissociation of the simplest polyatomic molecule, H_3^+. The use of dissociative states provides information on the orientation-dependent effects.

Although more than 70 years have passed since its discovery by Thompson[3] in 1912, our understanding of H_3^+ is still incomplete. We know that H_3^+ has an equilateral triangle structure as confirmed by Gaillard *et al.*[4] in their thin-foil-induced dissociation experiment. We also know the binding energies of H_3^+ as determined by Goh and Swan.[5] However, the only spectroscopic information on this fundamental ion is the recent observation of its infrared spectrum of the rovibrational transitions in the active degenerate ν_2 infrared band by Oka.[6] Also, cross sections for L_α production have been measured for H_3^+ incident on H_2 and He by Dunn *et al.*[7] without any attempt at explaining possible excitation mechanisms. Differential cross sections for metastable H(2*s*) production for H_3^+ incident on H_2, Ar, and N_2 were determined by Thomas *et al.*[8] Balmer emission yields produced by H_3^+ ions passing through thin carbon foils and noble gases were measured by Kobayashi and Oda,[9] and Bobashev *et al.*,[10] respectively. Also, the absolute cross sections for the production of H(3*s*) from fast H_3^+ were given by Hughes *et al.*[11] Finally, Peart and Dolder[12] investigated the production of deexcited H_3^+ ions and measured the absolute cross sections of the formation of H^+ by collisions between electrons and H_3^+. On the theoretical side, we have a long list which includes the *ab initio* calculation of its vibration spectrum by Carney and Porter,[13] the energy surfaces of the ground state by Carney and Porter[13,14] and also by Dykstra and Swope[15] and of several electronically excited states by Schaad and Hicks.[16] There is also some theoretical and experimental evidence that it is an important catalyst in the stellar medium.[17–20] It is well known that due to the rapid rate ($k = 2.1 \times 10^{-9}$ cm^{3}s^{-1}) of the reaction

$$H_2^+ + H_2 \rightarrow H_3^+ + H$$

there are large concentrations of H_3^+ in dense stellar clouds. Thus, H_3^+ provides one of the important mechanisms of molecular formation in stellar medium according to the reaction

$$H_3^+ + X \rightarrow XH^+ + H_2 ,$$

where X may be CO, N_2, H_2O, NH_3, Si, S, H_2S, etc., or even some larger molecules such as CH_2CHCCH. Seventy-seven reactions involving H_3^+ in stellar clouds were determined with their rate coefficients by Suzuki.[20]

II. EXPERIMENTAL PROCEDURE AND RESULTS

The specific experiment we have performed, and report on here, is the measurement of the polarization of L_α radiation in coincidence with the scattered H_2^+ resulting from the collision process:

$$H_3^+ + He \rightarrow (H_3^+)^* + He \rightarrow H_2^+ + H(n=2) + He .$$

Cross-sections differential in H_2^+ scattering angle for this process have been measured and reported[21] previously, without any L_α polarization analysis. Details of the apparatus have been discussed elsewhere.[22] A duoplasmatron ion source, an analyzing magnet, and electrostatic focusing lenses provide a beam of H_3^+. The H_3^+ is produced in the lowest vibrational state due to the vibrational deexcitation collisions with H_2 in the source that is run at a pressure of 0.3–0.5 Torr. Experiments by Leventhal and Friedman,[23] and also by Peart and Dolder[12] indicate that at these operational pressures the H_3^+ ion leaves the

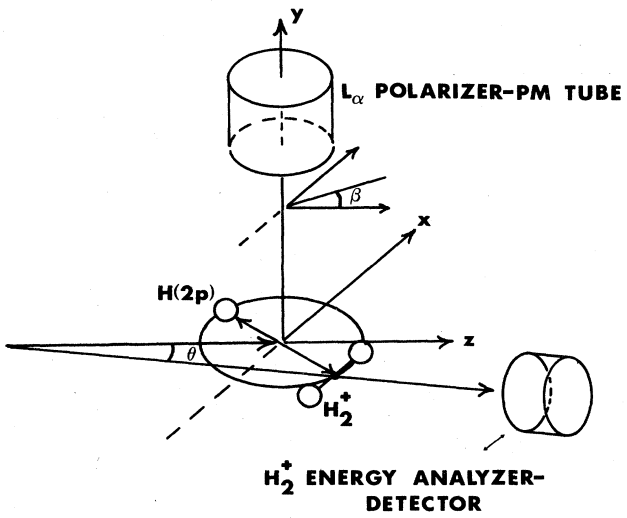

FIG. 1. Schematic arrangement for the H_2^+-L_α coincidence measurement for incident H_3^+ ions.

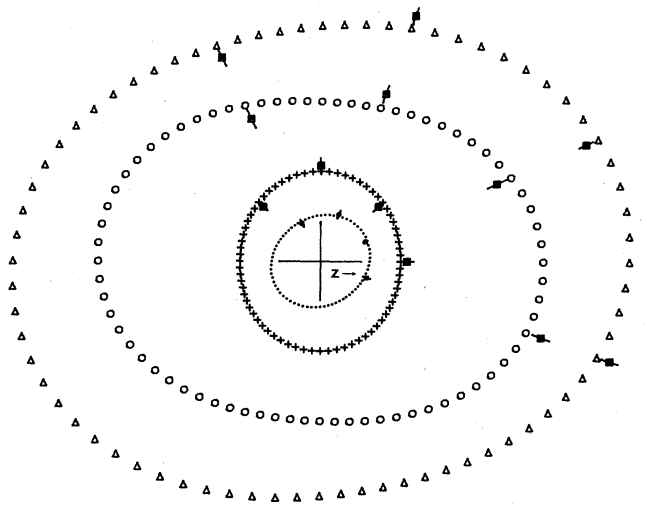

FIG. 2. Variations of $I(\beta)$ as a function of the H_2^+ scattering angle θ. △ for $\theta=1.0°$, ○ for $\theta=1.25°$, × for $\theta=1.5°$, and ● for $\theta=1.75°$. The z axis is the beam direction and different radii for different angles are to scale.

source in its vibrational ground state, a symmetric "breathing" mode. Results of the experiment reported later in this paper are also consistent with the H_3^+ being in this lowest vibrational state. A needle gas jet produces the gas target (He). The scattered charged particles are energy analyzed by a 90°-cylindrical electrostatic energy analyzer and detected by an electron multiplier. The L_α photons emitted perpendicular to the scattering plane are analyzed by a LiF Brewster-angle polarizer and observed by a solar-blind photomultiplier. The scattering plane is defined by the momenta of the incident H_3^+ beam and the H_2^+ dissociation product as shown in Fig. 1.

For a given H_2^+ scattering angle θ, L_α intensities $I(\beta)$ are determined by coincidence measurements for specific polarization angles β. The total integration time for each coincidence-data point varied from 18 h for 1° H_2^+ scattering angle to 134 h for 1.9° H_2^+ scattering angle. Figure 2 shows the variations of $I(\beta)$ as a function of the H_2^+ scattering angle θ along with a least-squares fit of the data to a generalized dipole-intensity pattern. In Figs. 3(a) and 3(b) we present the polar plots of $I(\beta)$ for $\theta=\pm1.25°$ and $\pm1.5°$, respectively, each normalized to unity for purposes of clarity. An inspection of these polar plots reveals that there is an abrupt change of the shape from $\theta=1.25°$ to 1.5°. In Sec. III we will attempt to explain this behavior and see how it can contribute to our understanding of the excitation of H_3^+ and subsequent dissociation into H_2^+ and $H(2p)$.

III. DISSOCIATION PROCESSES

For the incident H_3^+ beam energy of 4.83 keV, the collision duration ($\sim10^{-16}$ s) is a factor of 10 smaller than the dissociation time ($\sim10^{-15}$ s). The collision time is much less than either the photon decay of $H(2p)$ ($\sim10^{-9}$ s), or the precession time of the angular momentum ($\sim10^{-10}$ s), or the nuclear rotation period of the molecule ($\sim10^{-13}$ s). Therefore, the rotational motion can be considered as "frozen" during the dissociation.[24] The above considerations also mean that, for our energy, the electronic excitation of H_3^+ can be considered as resulting from Franck-Condon transitions. Finally, for 4.83-keV

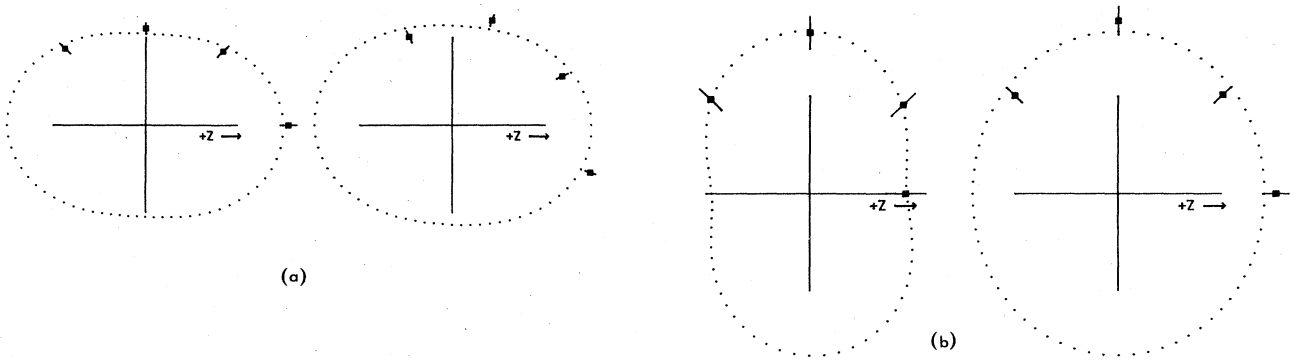

FIG. 3. (a) $I(\beta)$ for $\theta=\pm1.25°$, normalized to unity. (b) $I(\beta)$ for $\theta=\pm1.5°$, normalized to unity. The z axis shows the direction of the incident beam.

collision energy, reported here, the momentum transfer is small for the vast majority of H_3^+ ions and the deviation of the molecular center of mass negligible.[25] Although the importance of the molecular center-of-mass (c.m.) deflection after electronic excitation processes in collisions at low keV energies is not well established for H_3^+, one can gain some insight by considering the c.m. deflection of H_2^+. For 10-keV H_2^+ on several target gases, Baldreich, Lotz, and Ewald[26] find experimentally that a negligible c.m. deflection is observed for the electronic excitation of the H_2^+ ions leading to dissociation. Assuming that the H_3^+ and H_2^+ are similarly deflected, the c.m. deflection of H_3^+ at 4.83 keV is also negligible. Thus, the internal potential energy above the dissociation limit of $H_2^+ + H^*$ and the initial orientation of H_3^+ determine, to a good approximation, the momenta of the fragments in the laboratory frame.

The results presented in Figs. 3(a) and 3(b) suggest that the alignments of the resulting H^*, which emit the L_α radiation, are different in the two cases and correspond to different m_1 values of the excited state. The m_1 values depend on the choice of the orientation of the quantization axis. In the following discussion, we will use the line which joins the excited H atom to the center of mass of the H_2^+ ion as the quantization axis. For a given kinetic energy of the dissociation products, the maximum laboratory scattering angle is obtained when the c.m.-to-c.m. axis of H_2^+-H^* system is perpendicular to the beam direction. Using this perpendicular c.m.-to-c.m. axis as the axis of quantization, Fig. 2 shows that, for $\theta \leq 1.25°$, $I(\beta)$ has the dominant characteristics of a $2p_{\pm 1}$ state while for $\theta > 1.25°$ it shows the characteristics of a $2p_0$ state.

We can understand the data in terms of the abrupt change in the excited H_3^+ state contributing to the signal. To do this, we first consider the velocity vector diagram of the dissociation process as shown schematically in Fig. 4. The vectors $\mathbf{V}_0$ and $\mathbf{V}_L$ denote the velocity of the c.m. of H_3^+ and the laboratory velocity of H_2^+, respectively. In anticipation of our results we note that the radius V_1 of the smaller circle is equal to the velocity of H_2^+ produced by the dissociation $H_3^+ \rightarrow H_2^+ + H(2p_{\pm 1})$. Similarly, the dissociation $H_3^+ \rightarrow H_2^+ + H(2p_0, 2s)$, as we shall see, is associated with the radius V_2 of the larger circle.

Since the symmetry and nodal structure of the dissociation products reflect the nodal structure of the excited molecular states, we can relate the measured polarization to states of the H_3^+ molecule having D_{3h} symmetry. The energy eigenvalues of these states have been calculated by Schaad and Hicks,[16] and are shown in Fig. 5. In Fig. 6,

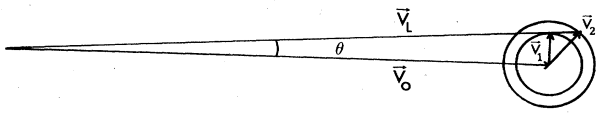

FIG. 4. The velocity vector diagram of the dissociation process. $\mathbf{V}_0$ and $\mathbf{V}_L$ denote the velocity of the c.m. and the laboratory velocity of H_2^+, respectively. The radii of the circles are equal to the velocities of H_2^+ produced by the reactions $H_3^+ \rightarrow H_2^+ + H(2p)$ (small circle) and $H_3^+ \rightarrow H_2^+ + H(2s)$ (large circle) in the c.m. of the H_3^+.

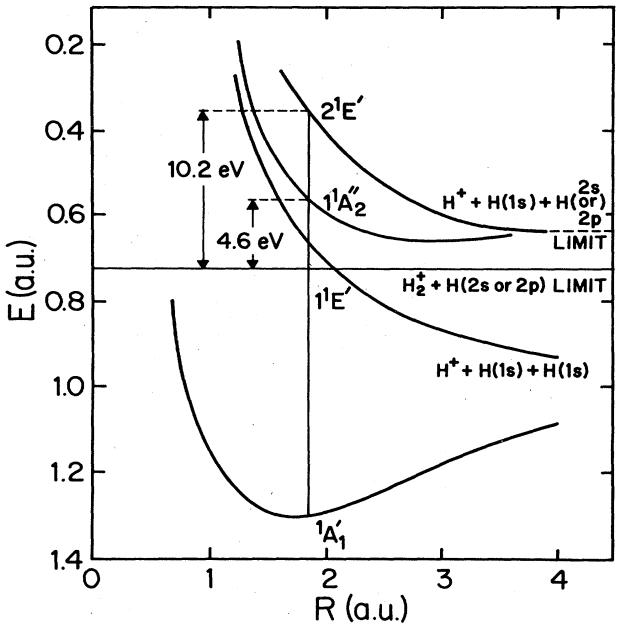

FIG. 5. Relevant H_3^+ states for D_{3h} symmetry (equilateral triangle structure). R is the length of the side of the triangle. These curves are only used for the excitation process where the shape of the H_3^+ is still an equilateral triangle.

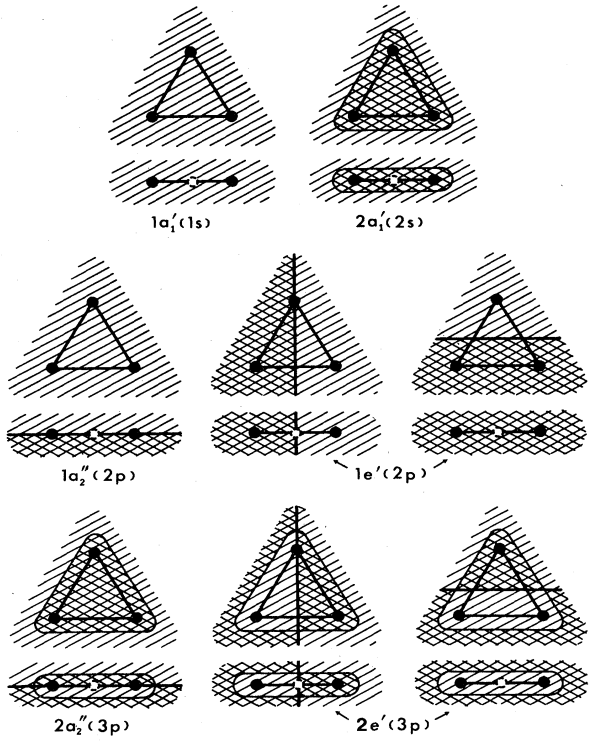

FIG. 6. The nodal structure of selected orbital functions of H_3^+ molecule in D_{3h} configuration. For each MO, the projections parallel and perpendicular to the H_3^+ plane are shown. The nodal surfaces are denoted by the heavier solid lines and the sign of the wave functions is marked by simple (+ sign) or cross hatching (− sign).

we also present the nodal surfaces of the relevant single-electron orbital functions of H_3^+ in D_{3h} configuration as given by Herzberg[27] and adopt the usual group-theoretical notation to label the states (capital letters) and the orbitals (lower-case letters). The atomic orbitals, given in parenthesis in Fig. 6, are the united-atom limit of the respective molecular orbitals.

Thus, we interpret the abrupt change in the polarization behavior between $\theta=1.25°$ and 1.5° as resulting from a change in the $(H_3^+)^*$ state contributing the maximum amount to the coincidence signal. For $\theta \leq 1.25°$ the transformation of velocities from the laboratory frame to the center-of-mass system gives a total maximum c.m. kinetic energy of approximately 4.6 eV, this being related to V_1 of Fig. 4. Also, for $\theta=1.25°$, the data presented in Fig. 3(a) shows that the electronic wave function is aligned with the major axis perpendicular to the quantization axis. Therefore, the polarization data suggest that, for the case of L_α emission, H_3^+ is excited mainly to a dissociative state with $H_2^+ + H(2p_{\pm 1})$ as the separated-atom limit. Schaad and Hicks[16] identify this state as $1^1A_2''[1a_1'(1s)1a_2''(2p)]$ of H_3^+ in D_{3h} symmetry. After the initial excitation, the D_{3h} symmetry (equilateral triangle) is broken and $1^1A_2''$ correlates with the $1^1A''$ state in C_s geometry (unequal-sided triangle). The vertical line on Fig. 5 shows the Franck-Condon transitions at the internuclear separation of 1.87 a.u.

At $\theta > 1.25°$ the above-mentioned dissociative state is not observed. The evidence for this, is the abrupt change in the polarization symmetry. The observed polarization is characteristic of the state which correlates with $H_2^+ + H(2p_0,2s)$ in the separated limit. This state, also calculated by Schadd and Hicks,[16] is the $2^1E'[1a_1'(1s)2e'(3p)]$ of H_3^+ in D_{3h} geometry. In C_s configuration, this state splits into two energy surfaces and the lower component correlates with $5^1A'$, dissociating into $H_2^+ + H(2s)$. Stark mixing of $H(2s)$ with $H(2p_0)$ state produces the L_α with $m_l=0$ character. The total maximum c.m. kinetic energy above the dissociation limit, that can be obtained from this state, is 10.2 eV. The vector diagram of Fig. 4 predicts that at $\theta > 1.86°$, one should not observe a large number of coincidences because the transformation of velocities from the c.m. to laboratory frame makes it energetically impossible to observe any coincidence signal produced by $2^1E'$ state for scattering angles $\theta > 1.86°$. This is confirmed by our measurements, for beyond $\theta=1.9°$, the H_2^+-L_α coincidence rate drops to zero.

IV. EXCITATION MECHANISM WITHIN QUASIDIATOMIC PICTURE

We can interpret our results in terms of the geometry of the excited-state wave functions and the dynamics of the collision using the independent-particle model within the quasidiatomic picture.[1,2]

Because of the near "atomiclike" character of the ground and low-lying excited-state wave functions of H_3^+ (Refs. 27 and 28), one can attempt to use a quasidiatomic picture to construct a correlation diagram that would provide a qualitative picture of the behavior of the diabatic electronic states of the H_3^+-He collision system. For example, if one considers the H_3^+ excited states $1e'$ and $1a_2''$ as shown in Fig. 6, they are essentially "p-like" in their nodal structure (p_x,p_y,p_z), with $1e'$ being doubly degenerate. Thus an appropriate linear combination of these orbitals can be used to construct an approximate set of p-like orbitals $p_{x'}$,$p_{y'}$,$p_{z'}$. Then using the c.m.-to-c.m. vector between H_3^+-He as the quantization axis (say z'), approximate (MO) orbitals can be constructed from linear combinations of "atomiclike" orbitals of H_3 and atomic orbitals of He. Extrapolations of diabatic states to close c.m.-to-c.m. distances are made by conserving the number of radial nodes according to Barat and Lichten,[29] and noting that the nodal structure of $1e'$ and $1a_2''$ is conserved when all three protons are brought together to form Li-like orbitals. Thus, the energy-level sequence of the "united-molecule limit" is approximated by B and the separated-system limit by H_3 and He.

It is also possible to define "σ-like" or "π-like" quasidiatomic orbitals by their shape and nodal structure, in analogy with diatomic MO. This would be equivalent to taking the projection of the quasidiatomic MO angular momentum on the line which joins the center of H_3^+ to He, as an approximate good quantum number. We denote the first "σ-like" quasidiatomic MO by $1q\sigma$, the first "π-like" by $1q\pi$, etc. This nomenclature is used to label the quasidiatomic molecular orbitals of Fig. 7. Figure 7 shows a semiquantitative quasidiatomic correlation diagram for the H_3-He system, drawn in the manner outlined above. Instead of using straight lines joining the separated and the united-atom (UA) limits, the curves are drawn at large c.m.-to-c.m. separations as straight horizontal lines with significant curvature occurring at smaller c.m.-to-c.m. distances. Since H_3 is unstable in its ground state, the energies of ground and excited states are not well known. Still, in the absence of any measurements, one can use the calculation by Kulander and Guest[30] to determine the $1a_1$ ground-state orbital and the $2a_1$ excited orbital in C_{2v} geometry. At the equilibrium separation of H_3^+, $1a_1$, and $2a_1$ orbitals correlate with $1a_1'$ and $1e'$ orbitals of D_{3h} symmetry, respectively. At this internuclear separation, the energy difference between $(1a_1^2 2a_1)$ and $(1a_1 2a_1^2)$ states of H_3 in C_{2v} configuration, can be used to determine the energy difference between $1a_1'$ and $1e'$ orbitals of H_3 in D_{3h} geometry. This difference is 16.2 eV. Kulander and Guest[30] also plotted on the same graph the $H_3^+(1a_1^2)$ ground-state energy in C_{2v} symmetry. Again at the equilibrium separation of H_3^+, the energy separation between $(1a_1^2 2a_1)$ of H_3 and $(1a_1^2)$ of H_3^+ gives the location of the $2a_1$ level as -5.94 eV. Hence, $H_3(1a_1')$ is 2.33 eV above He($1s$) on the correlation diagram. It should be noted here that if one uses the $1a_1'$ energy level of the H_3^+ ion, $1s$ of He, and $1a_1'(1s)$ of H_3^+ would be swapped. Swappings may also occur upon bond-length stretch or compression. But neither of these would change the fact that $1a_1'$ undergoes the promotion since this process is unambiguously determined by the coincidence signal. In the case of these swappings, a possible mechanism to interpret our results would be similar to K-vacancy sharing when the collision partners separate,

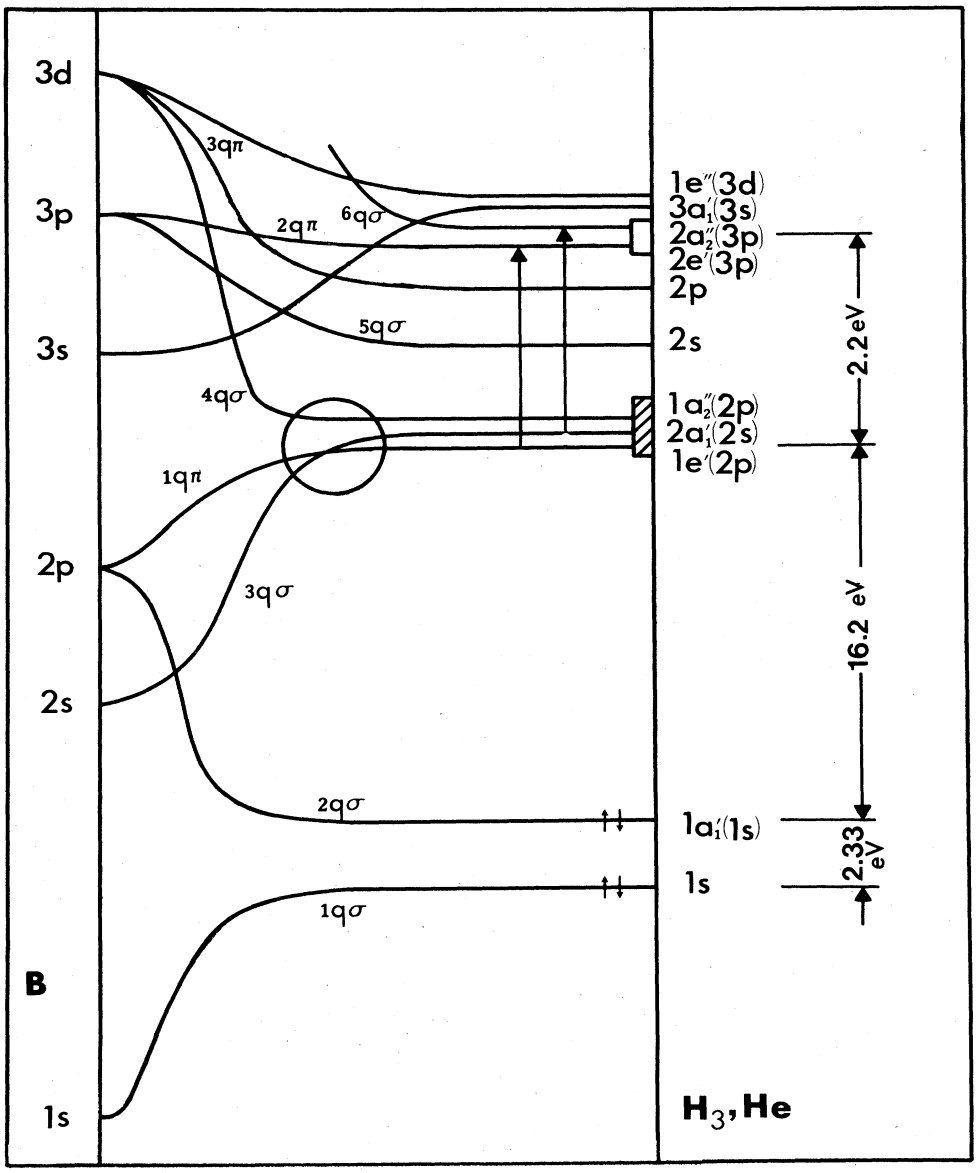

FIG. 7. Quasidiatomic MO correlation diagram for the H_3-He system. The small arrows represent the initially occupied orbitals. The energy separations of higher levels are greatly exaggerated.

due to the closeness of the $1q\sigma$ and $2q\sigma$ orbitals at large distances.

In the literature, there exist few experimental[31] and theoretical[32,33] works for the excited-energy levels of neutral H_3. The experimentally observed lines[31] are in good agreement with the theoretically calculated excitation energies.[32,33] Within the quasidiatomic approximation, $1e'(2p)$ and $1a_2''(2p)$ orbitals ($\sim$2.5 eV apart), which have roughly an atomic "$2p$-like" symmetry, are taken to have the same energy. Similarly, $2e'(3p)$ and $2a_2''(3p)$ ($\sim$0.4 eV apart) are nearly degenerate. The energy separation of higher levels is greatly exaggerated on the diagram to improve the readability.

As indicated, we have used the energies of the neutral species H_3—He to construct an MO diagram that represents the independent-particle energies of the system. The manner in which one does this is open to many questions.[34,35] The essential feature we require of the MO diagram is that it describes the approximate nodal character and behavior of the electronic wave function during the diabatic collision.

In a collision system as described here, the initial nodal character is determined at large c.m.-to-c.m. separation, with the quasidiatomic MO's being approximated linear combinations of $H_3(1a_1')$ and He($1s$) orbitals. The wave functions of particular interest are those associated with the $1q\sigma$ and $2q\sigma$ MO's of Fig. 7. The $1q\sigma$ state correlates with the lowest state of the united system. The $2q\sigma$

MO is characterized by a wave function having a nodal surface curved toward the more tightly bound and less extended He. This MO correlates to the $2p_{z'}$ state of the united system, crossing the $3q\sigma$ state with large probability in diabatic collisions. At the united-atom (UA) limit the $2p_{z'}$ nodal surface is a plane, since we are using an atomic representation. One characteristic of diabatic collisions is that the electronic wave function of the system tends to preserve its nodal character; this is manifested, in the present system, by the curve crossing of the diabatic states with large probability and the $2q\sigma$ correlating with $2p_{z'}$ at the UA limit.[36] However, at the same time, the nodal surface will tend to be curved near the UA limit, since we have an asymmetric diabatic system. This curved surface at the UA limit can approximately be represented by a mixture of $2p_{z'}$ and $2s$ states. Stated another way, at the $2q\sigma$ to $3q\sigma$ crossing, some amplitude is drained off to the $2s$ state near the UA limit. Thus, near the UA limit, the excited system is represented by a mixture of $2s$- and $2p_{z'}$-like functions thereby retaining the initial curved nodal surface characteristic.

A second well-known phenomenon that occurs is that at sufficiently high rotational speeds of the c.m.-to-c.m. axis, the electron-charge cloud tends to get left behind or "frozen" in space. This phenomenon can occur in any collision system: atom-atom, atom-molecule, or molecule-molecule. It is a dynamical effect that occurs because the electron wave function cannot keep up with the rapidly rotating c.m.-to-c.m.-axis frame. Bates and McCarroll[37] specify the limiting conditions where this is most likely to occur for diatomic collisions.

The problem then becomes one of describing this "leaving behind" or "freezing" of the electron wave function for a complicated system such as H_3^+-He. The function of particular concern to us here is the one belonging to the state labeled $2q\sigma$ in Fig. 7, the nodal character of which was established at large c.m.-to-c.m. distances. Viewed in the rotating c.m.-to-c.m.-axis frame, the "frozen" nodal surface is rotating. This rotation can be approximately described in the c.m.-to-c.m. frame by an appropriate mixing of nearly degenerate wave functions, as in diatomic collisions.[38]

Referring to Fig. 7, where the rotating coordinate-system functions are represented in the quasidiatomic approximation, this freezing is approximated by a mixing of the functions describing the $2q\sigma$ and $1q\pi$ states. This is generally called rotational coupling. Thus, we describe the initial phase of the collision by a promotion of the $2q\sigma$ level to the $1q\pi$ level by rotational coupling and a population of the $3q\sigma$ state because of the tendency to preserve the wave function shape. The degree to which both of these physical effects occur will depend upon the relative velocity, the impact parameter, and the details of the MO curves.

As the collision proceeds, the $q\sigma$ and $q\pi$ states uncouple at about the same c.m.-to-c.m. separation they began coupling, with a finite amplitude for the system proceeding back along the $2q\sigma$, $1q\pi$, and $3q\sigma$ states. The presence of $1q\pi$ and the further mixing of the $3q\sigma$ and $4q\sigma$ levels on the outgoing channels allows for the population of the $H_3[2a_1'(2s)]$, $H_3[1a_2''(2p)]$, and $H_3[1e'(2p)]$ orbitals. It must be emphasized that only the $1a_2''$ orbital leads to the observed $H_2^+ + H(2p)$ final products.

It should also be emphasized that within the quasidiatomic picture the $2a_1'(2s)$, $1a_2''(2p)$, and $1e'(2p)$ orbitals are considered to be degenerate. And, since the $1q\pi$-, $3q\sigma$-, and $4q\sigma$-orbital symmetries are defined relative to the c.m.-to-c.m. axis, the exact H_3^+ state excited will depend upon its orientation relative to this final axis, which, in this case, is the beam direction. The subsequent dissociation behavior of the excited H_3^+ will depend upon the specific orbital excited, that is, $2a_1'(2s)$, $1a_2''(2p)$, etc.

Since for the observed dissociating H_2^+-$H(2p)$ system, we can pinpoint when the H_2^+-$H(2p)$ axis is perpendicular to the beam direction, we will consider only this case. Specifically we consider only the three orientations as shown in Fig. 8.

First we consider the H_3^+ orientation as shown in Fig. 8(a), i.e., molecular plane perpendicular to the beam direction, with H_2^+ going in the y' direction upon dissociation.

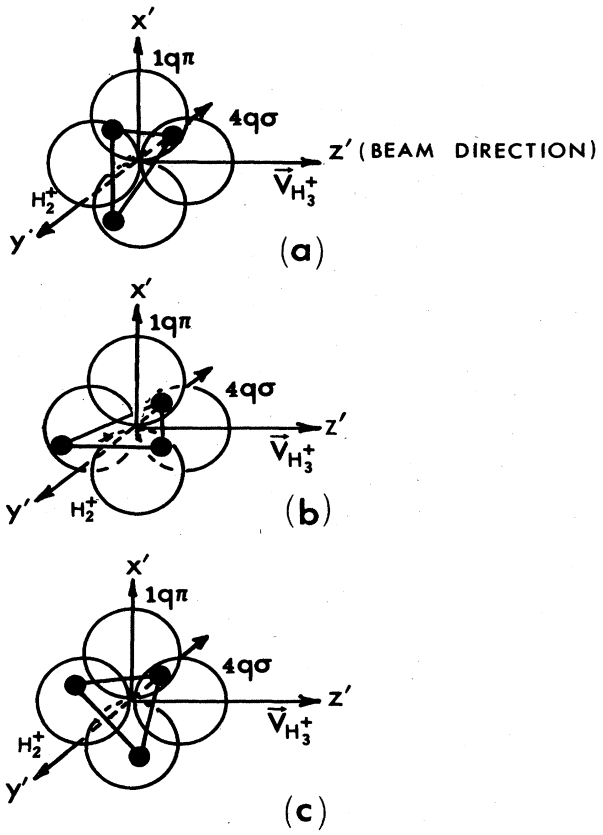

FIG. 8. Orientation dependence. The L_α observation direction is as shown in Fig. 1. H_3^+-He c.m.-to-c.m. axis is large and parallel to the beam direction. (a) Molecular plane is perpendicular to the beam direction. For this orientation, $4q\sigma$ tends to $1a_2''$ and $1q\pi$ to $1e'$ orbitals of H_3^+. (b) Molecular plane is parallel to the beam. In this case, $4q\sigma$ tends to $1e'$ and $1q\pi$ to $1a_2''$ orbitals of H_3^+. (c) Molecular plane has an intermediate orientation. $4q\sigma$ and $1q\pi$ can be approximately represented by linear combinations of $1e'$ and $1a_2''$ orbitals of H_3^+.

At large c.m.-to-c.m. separation, the $4q\sigma$ and $1q\pi$ states tend to $2p_{z'}$-like and $2p_{x'}$-like orbitals, respectively; these are shown schematically in Fig. 8(a). In the H_3^+ frame these are represented by $1a_2''$ and $1e'$ orbitals, respectively. Only the state associated with the $1a_2''$ orbital decays to $H_2^+ + H(2p)$. The L_α polarization pattern of the radiation emitted in the x' direction (our observation direction) would be preferentially polarized in the z' direction.

For the orientation shown in Fig. 8(b), i.e., molecular plane parallel to the beam, with H_2' going in the y' direction upon dissociation, the $4q\sigma$ and $1q\pi$ orbitals are represented in the H_3^+ frame by $1e'$ and $1a_2''$, respectively. The $H(2p)$ state formed in the decay of $1a_2''$ is aligned along the x direction, thus the L_α-polarization pattern from this would be a small circle. Without the precession, due to the spin-orbit interaction, the observed polarization intensities would be zero. From Fig. 3(a), we find for $\theta = 1.25°$ a measured polarization pattern preferentially aligned along the z direction, suggesting that our observations are more sensitive to the H_3^+ orientation shown in Fig. 8(a). For more arbitrary orientations, the c.m.-to-c.m. orbitals $4q\sigma$ and $1q\pi$, shown in Fig. 8(c), can be approximately represented by linear combinations $1e'$ and $1a_2''$ orbitals of H_3^+.

Since, for any one collision, the excitation to $4q\sigma$ and $1q\pi$ is coherent, we can visualize the excitation of H_3^+ as resulting from placing a planar node in the wave function, with the orientation depending upon the relative amplitudes and phases of $4q\sigma$ and $1q\pi$.

Within this model, additional nodes can be created through additional σ-σ and π-π couplings, due to the small resonance defects of the nearly parallel outgoing energy states.[39,40] These are shown by arrows in Fig. 7 between $1q\pi$ and $2q\pi$, and $4q\sigma$ and $6q\sigma$. This leads to $2a_2''$- and $2e'$-orbital excitation. Here again, the excitation depends upon the H_3^+ orientation, with the $2E'$ state dissociating to $H_2^+ + H$ $(2s,2p_0)$. Our measured polarization pattern at $\theta = 1.5°$ is indeed characteristic of $H(2p_0)$ excitation.

V. CONCLUSION

We have measured the L_α polarization in coincidence with the scattered H_2^+ for 4.83-keV $H_3^+ + He$ collision-induced dissociation process. The preferential alignment of the observed $H(2p)$ and the change of this alignment with H_2^+ scattering angle allow an identification of the H_3^+ states that are excited. When the H_2^+-$H(2p)$ axis is perpendicular to the beam direction, the observed L_α signal comes preferentially from the case when the H_3^+ plane is perpendicular to the beam direction, for the dissociation of $1A_2''$ state. No similar statement can be made for the dissociation of the $2E'$, since the H_2^+-$H(2p_0)$ system produces the same polarization pattern for arbitrary rotations about the H_2^+-$H(2p_0)$ axis. These observations are independent of any proposed excitation mechanisms.

Despite its simplicity, a quasidiatomic model incorporating simple correlation diagrams provides a reasonable description of the changing nodal structure of the wave functions during the collision.

ACKNOWLEDGMENTS

We are grateful to Professor J. Macek for many stimulating discussions, and to Professor G. Gallup for communicating his unpublished calculations on H_3^+. The support of this work by the National Science Foundation through a grant is gratefully acknowledged.

[1]D. Dowek, D. Dhuicq, V. Sidis, and M. Barat, Phys. Rev. A **26**, 746 (1982).
[2]D. H. Jaecks, O. Yenen, M. Natarajan, and D. Mueller, Phys. Rev. Lett. **50**, 825 (1983).
[3]J. J. Thompson, Philos. Mag. **24**, 209 (1912).
[4]M. J. Gaillard, D. S. Gemmel, G. Goldring, I. Levine, W. J. Pietsch, J. C. Poizat, R. J. Ratkowski, J. Remilleux, Z. Vager, and B. J. Zabrowsky, Phys. Rev. A **17**, 1797 (1978).
[5]S. C. Goh and J. B. Swan, Phys. Rev. A **24**, 1624 (1981).
[6]T. Oka, Phys. Rev. Lett. **45**, 531 (1980).
[7]G. H. Dunn, R. Geballe, and D. Pretzer, Phys. Rev. **128**, 2200 (1962).
[8]E. W. Thomas, R. L. Fitzwilson, I. Savers, and J. C. Ford, J. Chem. Phys. **63**, 4092 (1975).
[9]H. Kobayashi and N. Oda, J. Phys. Soc. Jpn. **51**, 2715 (1982).
[10]S. V. Bobashev, E. P. Andreev, and V. A. Ankudinov, Zh. Eksp. Teor. Fiz. **45**, 1759 (1963) [Sov. Phys.—JETP **18**, 1205 (1964)].
[11]R. H. Hughes, D. B. Kay, C. A. Stigers, and E. D. Stokes, Phys. Rev. **167**, 26 (1968).
[12]B. Peart and K. T. Dolder, J. Phys. B **7**, 1567 (1974).
[13]G. D. Carney and R. N. Porter, J. Chem. Phys. **65**, 3547 (1976).
[14]G. D. Carney and R. N. Porter, J. Chem. Phys. **60**, 4251 (1974).
[15]C. E. Dykstra and W. C. Swope, J. Chem. Phys. **70**, 1 (1979).
[16]L. J. Schaad and W. V. Hicks, J. Chem. Phys. **61**, 1934 (1974).
[17]E. Herbst and W. Klemperer, Astrophys. J. **185**, 505 (1973).
[18]W. D. Watson, Rev. Mod. Phys. **48**, 513 (1976).
[19]A. Dalgarno and G. Black, Rep. Prog. Phys. **39**, 573 (1976).
[20]H. Suzuki, Prog. Theor. Phys. **62**, 936 (1979).
[21]D. L. Montgomery and D. H. Jaecks, Phys. Rev. Lett. **51**, 1862 (1983).
[22]R. H. McKnight and D. H. Jaecks, Phys. Rev. A **4**, 2281 (1971).
[23]J. J. Leventhal and L. Friedman, J. Chem. Phys. **50**, 2928 (1969).
[24]R. N. Zare, J. Chem. Phys. **47**, 204 (1967).
[25]J. Los and T. R. Govers, in *Collision Spectroscopy,* edited by R. G. Cooks (Plenum, New York, 1978).
[26]W. Baldreich, W. W. Lotz, and H. Ewald, Z. Phys. A **317**, 23 (1984).
[27]G. Herzberg, *Electronic Spectra of Polyatomic Molecules* (Van Nostrand, New York, 1966).
[28]A. Streitwieser, Jr. and P. H. Owens, *Orbital and Electron Density Diagrams* (Macmillan, New York, 1973).
[29]M. Barat and W. Lichten, Phys. Rev. A **6**, 211 (1972).
[30]K. C. Kulander and M. F. Guest, J. Phys. B **12**, L501 (1979).

[31]G. Herzberg, H. Lew, J. J. Sloan, and J. K. G. Watson, Can. J. Phys. **59**, 428 (1981).
[32]M. Jungen, J. Chem. Phys. **71**, 3540 (1979).
[33]R. L. Martin, J. Chem. Phys. **71**, 3541 (1979).
[34]Q. C. Kessel and B. Fastrup, *Case Studies in Atomic Physics* (North-Holland, Amsterdam, 1974), p. 140ff.
[35]J. Eichler, U. Wille, B. Fastrup, and K. Taulbjerg, Phys. Rev. A **14**, 707 (1976).
[36]W. Lichten, Phys Rev. **131**, 229 (1963).
[37]D. R. Bates and R. McCarroll, Adv. Phys. **12**, 39 (1962).
[38]F. J. Eriksen, D. H. Jaecks, W. de Rijk, and J. Macek, Phys. Rev. A **14**, 119 (1976).
[39]Y. N. Demkov, Zh. Eksp. Teor. Fiz. **45**, 195 (1963) [Sov. Phys.—JETP **18**, 138 (1964)].
[40]S. J. Pfeifer and J. D. Garcia, Phys. Rev. A **23**, 2267 (1981).